Impedance Analysis and Single-Channel Recordings on Nano-Black Lipid Membranes Based on Porous Alumina

Winfried Römer and Claudia Steinem
Institut für Analytische Chemie, Chemo- und Biosensorik, Universität Regensburg, 93040 Regensburg, Germany

ABSTRACT Ordered porous alumina substrates with pore diameters of 55 and 280 nm, respectively, were produced and utilized as a support to prepare membranes suspending the pores of the material. Highly ordered porous alumina was prepared by an anodization process followed by dissolution of the remaining aluminum and alumina at the backside of the pores. The dissolution process of Al_2O_3 at the backside of the pores was monitored by electrical impedance spectroscopy ensuring the desired sieve-like structure of the porous alumina. One side of the porous material with an area of 7 mm^2 was coated with a thin gold layer followed by chemisorption of 1,2-dipalmitoyl-*sn*-glycero-3-phosphothioethanol. The hydrophobic monolayer on top of the upper surface was a prerequisite for the formation of suspending membranes, termed nano-black lipid membranes (nano-BLMs). The formation process, and long-term and mechanical stability of the nano-BLMs were followed by electrical impedance spectroscopy indicating the formation of lipid bilayers with typical specific membrane capacitances of (0.65 $\pm$ 0.2) $\mu F/cm^2$ and membrane resistances of up to 1.6×10^8 Ω cm^2. These high membrane resistances allowed for single-channel recordings. Gramicidin as well as alamethicin was successfully inserted into the nano-BLMs exhibiting characteristic conductance states.

INTRODUCTION

Approximately one-third of all proteins of an organism comprising pores, ion channels, receptors, and enzymes are membrane associated. These proteins require a lipid bilayer for proper function, which makes it difficult to handle them. However, membrane proteins, and in particular ion channels and receptor proteins, are main drug targets, and thus, they have received widespread recognition for their application in biosensors, drug discovery, and protein/ligand screening. One approach to elucidate the functioning of ion channels is to reconstitute them into planar lipid bilayers formed across apertures in thin films, often Teflon of 5–25 μm with hole diameters of 0.1–1 mm (Mueller et al., 1963; Tien and Ottova, 2000). These membranes are, however, not suited for automation and miniaturization as required for biosensors and high-throughput screening assays for potential drugs. To produce apertures that can be used in chip technology, new strategies based on microfabricated apertures in silicon have thus been followed in the last years. Lipid membranes suspending 0.7–100-μm-large apertures manufactured in silicon were prepared with various techniques ranging from spreading lipids in an organic solvent to spreading and fusion of giant unilamellar vesicles (Cheng et al., 2001; Ogier et al., 2000; Osborn and Yager, 1995; Peterman et al., 2002; Schmidt et al., 2000). Typical long-term stability of these membranes was in the order of several hours. Similar stabilities were reported for lipid membranes formed on polycarbonate membranes with holes of 1 μm in diameter and microporous glass with hole sizes of 0.7 μm (Andreou and Nikolis, 1998; Favero et al., 2003, 2002; Nikolelis and Siontorou, 1995).

A different approach for constructing membrane biosensors is to use lipid bilayers immobilized on a solid support. These membranes can be prepared on various surfaces, i.e., glass, silicon, and mica, or on metal surfaces such as platinum or gold with almost arbitrary lateral dimensions (Purrucker et al., 2001; Sackmann, 1996; Steinem et al., 1996; Tien and Ottova, 1998). Surface attachment of the lipids is typically achieved following two different strategies, the deposition of Langmuir-monolayers or more easily by self-assembly techniques. The major advantage of this membrane type is its attachment to a solid support, resulting in long-term and high mechanical stability. Solid supported membranes can be accessed by a variety of sensitive surface analysis tools such as scanning probe microscopy, attenuated total reflection-infrared, quartz crystal microbalance technique, and surface plasmon resonance spectroscopy, as well as electrochemical methods provided that the support is electrically conducting. In principle, solid supported membranes enable one to rationally design biosensor devices for high throughput screening assays based on sophisticated micromachined chip technology. However, the applicability of these membranes is restricted by their close surface proximity, which limits or even prevents the incorporation of large transmembrane-spanning proteins. Approaches to extend the distance between solid support and lipid bilayer include polymer cushions and hydrophilic spacers tethering the bilayer to the support (Baumgart et al., 2003; Naumann et al., 2002; Raguse et al., 1998; Sackmann, 1996; Sackmann and Tanaka, 2000; Sengupta et al., 2003; Stora et al., 1999). The increased distance, however, still does not allow for a free ion movement. Moreover, in most cases solid supported membranes tend to be too permeable to permit the detection of single-channel activity. Only very recently, Vogel and co-workers reported on a hybrid bilayer immobilized on a gold surface that exhibits a very high membrane resistance of 7 MΩ cm^2 (Terrettaz et al., 2003).

Submitted May 30, 2003, and accepted for publication October 16, 2003.

Address reprint requests to Claudia Steinem, Tel.: +49-941-943-4548; Fax: +49-941-943-4491; E-mail: claudia.steinem@chemie.uni-regensburg.de.

0006-3495/04/02/955/11 $2.00

The aim of our work was to obtain a membrane system that is on the one hand attached to a solid support so that it can be applied in chip technology with the future perspective to obtain high-throughput screening assays based on electrochemical or surface sensitive methods. On the other hand, the membrane system should exhibit such high membrane resistances that it is suited for single-channel measurements. We present a membrane type being a hybrid between a solid supported membrane and a freestanding lipid bilayer, called nano-black lipid membrane (nano-BLM). A highly ordered porous substrate with tunable but very well-defined pore sizes of either 55 or 280 nm based on aluminum serves as the ''solid support''. The porous alumina substrate can be easily and reproducibly prepared in almost arbitrary lateral dimensions making this material well-suited for its application in biosensor devices. After formation of a closed alumina pore structure, opening of the pores from the backside, which is achieved by selectively removing the aluminum oxide of the pore bottoms, can be followed by means of impedance spectroscopy ensuring a sieve-like structure in which all pores are open. Lipid bilayers are prepared suspending the pores, whereas part of the membrane is supported by the alumina substrate. The as-prepared membranes exhibit high long-term stability as deduced from impedance analysis. Membrane capacitances indicate lipid bilayers suspending the pores, and membrane resistances are sufficiently high to allow for single-channel measurements. The insertion of gramicidin and alamethicin after formation of nano-BLMs corroborates the formation of single bilayers and shows the applicability of this membrane type for measurements of channel activity on a reasonable timescale.

MATERIALS AND METHODS

Materials

Aluminum substrates (thickness 0.5 mm, purity 99.999%) were purchased from Goodfellow (Goodfellow Cambridge Limited, Huntingdon, UK). 1,2-Dipalmitoyl-*sn*-glycero-3-phosphothioethanol (DPPTE) and 1,2-diphytanoyl-*sn*-glycero-3-phosphocholin (DPhPC) were obtained from Avanti Polar Lipids (Alabaster, AL). Gramicidin D, a mixture of the naturally occurring gramicidins A, B, and C as well as alamethicin, was obtained from Sigma-Aldrich (Taufkirchen, Germany). The water used was ion-exchanged and Millipore-filtered (Millipore Milli-Q-System, Molsheim, France, specific resistance $R > 18$ MΩ cm^{-1}, pH 5.5).

Preparation of porous alumina substrates

High purity aluminum foils (2×2 cm^2) cleaned in acetone and isopropanol, were first annealed under a nitrogen atmosphere at 500°C for 3 h. Then, the aluminum foils were electropolished three times in a mixture composed of sulphuric acid, phosphoric acid, and water (2:2:1, v/v/v) at 70°C for 40 s (Jessensky et al., 1998). Porous structures were obtained by anodizing the electropolished aluminum foils in acidic solutions. Anodization was conducted under constant cell potential using either aqueous oxalic (0.3 M) or phosphoric acid (5 wt %) as electrolyte. In case of phosphoric acid, porous alumina was obtained in a one-step anodization process. Aluminum was anodized at $T = 2$°C and $V = 160$ V for 48 h resulting in ordered pores at the bottom of the porous layer, whereas the top exhibits a rather nonordered pore structure. Pore depth depends on etching time and is reported to be 4–5 μm/h in phosphoric acid. In case of oxalic acid as electrolyte, hexagonally ordered pores on both sides of the porous membrane were obtained by a two-step anodization process. First, aluminum was anodized in 0.3 M oxalic acid at $T = 2$°C and $V = 40$ V for 3 h. Second, the oxide layer was removed by wet chemical etching in a mixture of phosphoric acid (6 wt %) and chromium (VI) oxide (1.8 wt %) at 60°C for at least 3 h (Li et al., 1998, 1999a,b). The remaining pattern on the aluminum substrate serves as a mask for the second anodization process using the same parameters as in the first step. Pores that are formed in the second anodization step are hexagonally ordered. Pore depth again depends on etching time and is reported to be 1–2 μm/h. After anodization, aluminum was removed by incubating the substrate in a saturated $HgCl_2$ or acidulated $CuCl_2$ solution resulting in a porous alumina membrane with closed pores at the backside (pore bottoms). To remove the alumina pore bottoms, the porous membrane was chemically etched at 30°C in 5 wt % phosphoric or 0.3 M oxalic acid solution (Li et al., 1998, 1999a,b).

Functionalization of alumina surfaces

Gold coating of the top or bottom surface of the porous alumina was achieved by sputtering titanium (5–10 nm) as an adhesive layer followed by a gold layer (25–70 nm) using a sputter coater with a thickness control unit (Cressington sputter coater 108auto, Cressington MTM-20, Elektronen-Optik-Service, Dortmund, Germany). The thickness of the titanium and gold layers, respectively, was properly adjusted according to the pore size to ensure that the pores are not filled with metal. The gold-coated surface was functionalized by incubating the porous alumina surface in a 1 mM ethanolic solution of DPPTE for at least 12 h, which renders the gold-coated surface hydrophobic. After thoroughly rinsing with ethanol and drying under a stream of nitrogen, the porous sample was mounted in the Teflon cell (Fig. 1).

Formation of nano-BLMs

Before forming the nano-BLMs, the surface surrounding the hole was primed with the phospholipid solution. A solution of DPhPC in pentane (5%

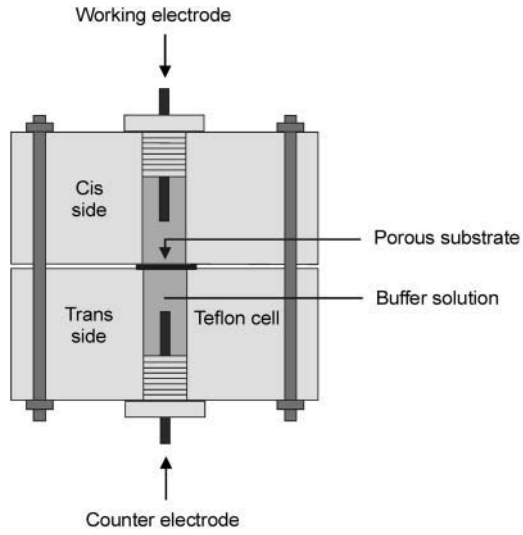

FIGURE 1 Schematic drawing of the Teflon cell used for electrochemical impedance analysis and single-channel recordings. Ag/AgCl electrodes were used for single ion channel measurements; platinized platinum or Ag/AgCl electrodes for impedance spectroscopy.

w/v) was applied to the orifice and then dried in a stream of nitrogen. Then, the substrate was vertically placed in the Teflon cell (Fig. 1) and the *cis* and *trans* compartments were filled with electrolyte solution. Ten μl of a DPhPC solution in *n*-decane (1% w/v) were painted over the DPPTE-functionalized surface oriented to the *cis* side.

Electrochemical impedance spectroscopy

Porous alumina substrates and lipid membrane covered porous alumina were investigated using electrical impedance spectroscopy. AC impedance analysis was performed using the impedance gain/phase analyzer SI 1260 and the 1296 Dielectric Interface (Solartron Instruments, Farnborough, UK) controlled by a personal computer. The absolute values of the impedance $|Z|(f)$ and the phase angles φ (f) between voltage and current were recorded within a frequency range of 10^{-2}–10^{6} Hz, with equally spaced data points on a logarithmic scale and with five data points per decade, which took ~12 min. All data were obtained at zero offset potential applying a small sinusoidal AC voltage of 30 mV to avoid nonlinear responses. Impedance data were recorded with the Solartron Impedance Measurement Software (Version 3.5.0) and analyzed using the software package ZView2.6b with Calc-Modulus data weighting. Electrochemical measurements were carried out using the Teflon cell as schematically depicted in Fig. 1. The cell consists of two identical compartments separated by the porous alumina substrate with an area of 7 mm^2 sealed by an O-ring. Platinized platinum and Ag/AgCl wires, respectively, immersed in the electrolyte solution on both sides, serve as working (*cis* compartment) and counter electrode (*trans* compartment). Electrochemical impedance measurements were performed in 0.1 M Na_2SO_4 and 0.5 M KCl, respectively. No differences in impedance spectra using those two types of electrodes were observed.

Single-channel recordings

Single-channel recordings were carried out in the Teflon cell (Fig. 1) equipped with two Ag/AgCl electrodes in the *cis* and *trans* compartment, which were connected to an Axopatch 200B patch-clamp amplifier (Axon Instruments, Foster City, CA) in capacitive or resistive feedback configuration. The *trans* compartment was connected to ground and all potentials in the *cis* compartment are given relative to ground. Data were filtered with a low-pass cutoff filter of 1 kHz. The analog output signal was digitized by an A/D converter (Digidata 1322A, Axon Instruments). Currents were recorded using pClamp 8.0 software (Axon Instruments) with a sampling rate of 5 kHz, while applying holding potentials V_h ranging between −150 and +150 mV. To avoid interference from electric fields during measurements, the electrochemical cell was placed in a Faraday cage set on a mechanically isolated support (Hanke and Schlue, 1993). Single-channel experiments were mainly performed in symmetrical nonbuffered solutions of 0.5 M KCl, in case of gramicidin single channels also in 0.5 M LiCl, and CsCl solution. Gramicidin D was incorporated into the nano-BLMs by adding the peptide dissolved in ethanol (10^{-6} M) to the electrolyte solution of both sides resulting in a nominal peptide concentration of ~10^{-8} M. Alamethicin was added to one side of the membrane after bilayer formation from a 10^{-5} M stock solution in ethanol leading to a final concentration of ~10^{-7} M.

RESULTS

Impedance analysis of the pore-opening process

After anodization of the aluminum substrates, porous alumina embedded in aluminum is obtained. First, aluminum has to be removed. This is achieved by oxidizing and completely dissolving it in either $HgCl_2$ or acidulated $CuCl_2$ solution, which takes ~20 min up to 3 h. Scanning electron microscopy (SEM) images of the bottom of the porous alumina clearly demonstrate that dissolution of aluminum in a saturated $HgCl_2$ solution takes longer but is much gentler than dissolution in $CuCl_2$ solution, which is a faster process but may result in a complete decomposition of the porous oxide layer.

Second, the aluminum oxide barrier layer needs to be fully removed to obtain a sieve-like structure, in which all pores are open on both sides. This is achieved by chemically dissolving aluminum oxide in acidic solutions. To follow the opening process and ensure that aluminum oxide at the backside of the pores is eventually completely removed, we performed impedance analysis. In Fig. 2 *A*, typical impedance spectra of a porous alumina membrane obtained

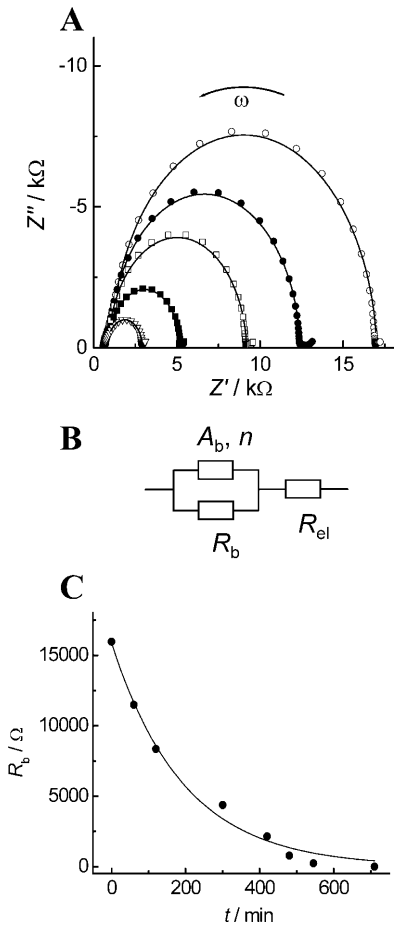

FIGURE 2 (*A*) Impedance spectra in a frequency range of 10^{-1}–10^{6} Hz of a porous alumina substrate obtained by anodization of an aluminum foil in phosphoric acid solution before and after several time periods in oxalic acid solution: (○) 0 min, (●) 60 min, (□) 120 min, (■) 300 min, and (∇) 420 min. The solid lines are the results of the fitting procedure with the equivalent circuit shown in Fig. 2 *B*. (*B*) Equivalent circuit composed of a parallel circuit of a *cpe*-element (A_b, n) and a resistance R_b in series to an ohmic resistance R_{el} representing the electrolyte solution. (*C*) Time course of the resistance R_b obtained from the impedance data during the pore opening process. The time course empirically follows a monoexponential decay (*solid line*) with a decay time τ of 195 ± 14 min.

by anodization in phosphoric acid solution followed by removing aluminum and aluminum oxide at the backside of the pores by oxalic acid treatment are depicted. The impedance spectra are characterized by a typical semicircle and can be modeled by an equivalent circuit composed of three elements (Fig. 2 *B*). The ohmic resistance R_{el} represents the electrolyte resistance, which is in series to a parallel circuit of a constant phase element (*cpe*-element) (A_b, n) and a resistance R_b characteristic for the aluminum oxide layer at the backside (de Laet et al., 1995). Fitting the parameters of the equivalent circuit to the data results in very good agreement between data and fit. R_b, A_b, and n can be readily extracted from the time-resolved impedance spectra. While incubating the porous alumina membrane in the acidic solution, R_b considerably decreases (Fig. 2 *C*), indicating a decrease in aluminum oxide thickness at the backside. The time course empirically follows a monoexponential decay with a decay time τ of 195 ± 14 min. During the dissolution process, A_b increases starting from a value of 47.4 nF until it disappears at the end of dissolution when all pores are open. For n, a slight decrease is observed from 0.99 to 0.93, which is still close to 1 implying that the parameter A_b can be viewed as the capacitive behavior of the aluminum oxide layer. After 710 ± 150 min, the electrical parameters of the oxide layer at the backside, R_b and A_b, cannot be detected anymore, indicative of a complete dissolution of the aluminum oxide at the backside of the pores. The impedance spectrum is only characterized by the ohmic resistance R_{el} of the bulk electrolyte and the capacitance of the counter electrode becomes discernable at low frequencies (see Fig. 4 *A*). The fact that only the resistance of the bulk electrolyte is detected by impedance analysis shows that the current solely flows through the pores, whereas the alumina columns are not detected by impedance spectroscopy.

The time period until the barrier oxide layer is completely dissolved depends on the porous alumina type and the used acidic solution. Removal of the backside aluminum oxide layer of porous alumina obtained from anodizing in phosphoric acid exhibits a decay time τ of 23 ± 4 min in phosphoric acid and of 195 ± 14 min in oxalic acid, whereas τ is 2.2 ± 0.3 min in phosphoric acid and 95 ± 17 min in oxalic acid when starting with porous membranes that were anodized in oxalic acid. The decay time τ of the monoexponential decay and the corresponding time periods required for completely opening of the pores are summarized in Table 1. From the obtained data, it was concluded that the most convenient and time-saving method is to anodize aluminum in phosphoric acid solution followed by aluminum dissolution in saturated $HgCl_2$ followed by pore bottom opening in phosphoric acid solution.

As oxalic and phosphoric acid simply dissolve aluminum oxide, the oxide layer at the backside is not selectively removed and as a result the procedure also leads to a widening of the pores. Thus, we performed SEM to fully characterize the material.

TABLE 1 Decay times τ and time periods of pore bottom opening of porous alumina in different acidic solutions

Etch process Pore bottom opening	τ/min	Time period*/min
Oxalic acid Oxalic acid	95 ± 17	340 ± 70
Oxalic acid Phosphoric acid	2.2 ± 0.3	14 ± 3
Phosphoric acid Phosphoric acid	23 ± 4	60 ± 12
Phosphoric acid Oxalic acid	195 ± 14	710 ± 150

*The time period is defined as the time until the impedance spectrum only shows the electrolyte resistance, indicating that all pore bottoms are dissolved.

SEM characterization of porous alumina substrates

SEM images of the backside of the alumina substrates after a thin gold layer was sputtered on the surface are shown in Fig. 3. Porous alumina substrates obtained after 48 h of anodization in phosphoric acid followed by aluminum dissolution in saturated $HgCl_2$ and pore bottom opening in phosphoric acid solution exhibit a mean pore size distribution of 280 ± 45 nm and a thickness of 195 ± 30 μm (Fig. 3 *A*), which translates to a pore growth rate of 4–5 μm/h. A surface porosity of 33 ± 4% was calculated by pixel analysis from the SEM images, which is in good agreement with the results of Gösele and co-workers (Li et al., 1998, 1999a,b; Nielsch et al., 2002). Porous alumina obtained by anodizing in 0.3 M oxalic acid for 96 h followed by aluminum dissolution in saturated $HgCl_2$ and pore bottom opening in phosphoric acid solution leads to a pore size distribution of 55 ± 8 nm, a thickness of 150 ± 20 μm, and a surface porosity of 60 ± 8% (Fig. 3 *B*). The growth rate is thus 1–2 μm/h.

Impedance analysis of the formation of nano-BLMs on porous alumina substrates

The most convenient and time-saving method is to anodize aluminum in phosphoric acid solution followed by aluminum dissolution in saturated $HgCl_2$ and pore bottom opening in phosphoric acid solution. Thus, we mainly used these substrates, and the results based on these substrates are discussed in more detail below. However, the same results were obtained for porous substrates obtained by anodizing aluminum in oxalic acid, which leads to smaller pores.

Before bilayer deposition, one side of the porous alumina substrate was covered with a thin gold layer, which allows for the chemisorption of thiol compounds. The phospholipid DPPTE was self-assembled on the gold surface, rendering it hydrophobic. After incubation with the thiol compound, the functionalized alumina substrates were investigated by impedance spectroscopy. Impedance analysis revealed that

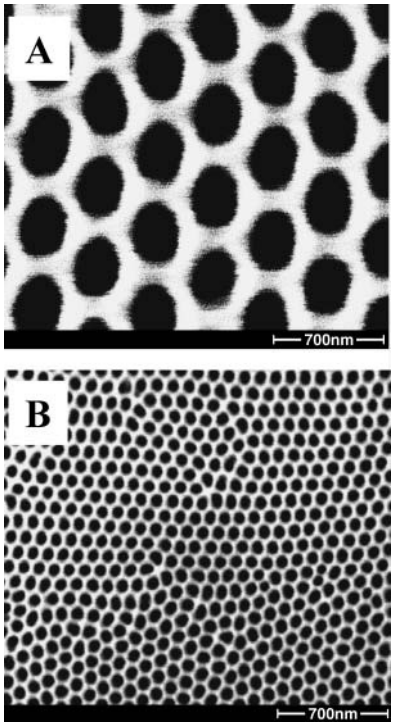

FIGURE 3 SEM micrographs (bottom views) of highly ordered anodic alumina layers anodized under different conditions. Anodization was conducted (*A*) in 5 wt % phosphoric acid at $T = 2$°C and $V = 160$ V and (*B*) in 0.3 M oxalic acid at $T = 2$°C and $V = 40$ V. The determined pore diameters are (*A*) 280 ± 45 nm and (*B*) 55 ± 8 nm.

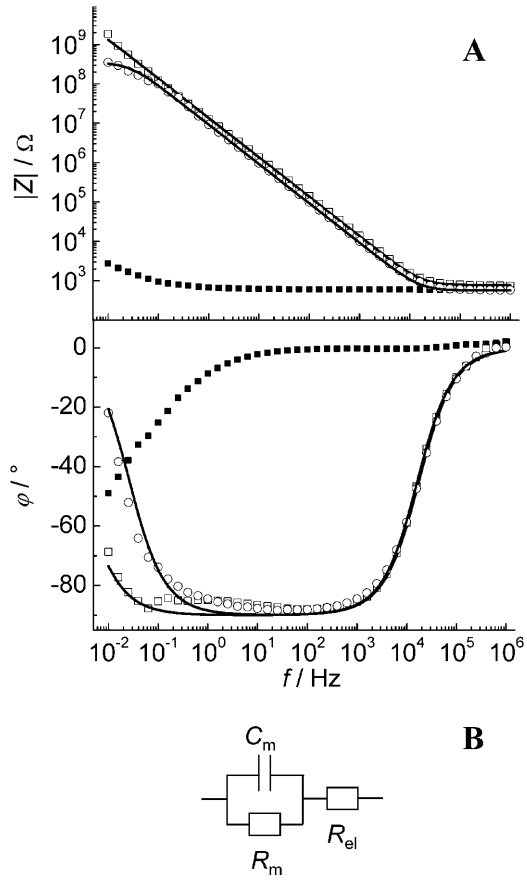

FIGURE 4 (*A*) Impedance spectra of gold-covered porous alumina membranes functionalized with a DPPTE-monolayer before (■) and after (□, ○) spreading of a lipid droplet across the porous alumina substrate. (□) An impedance spectrum obtained one day after formation of a nano-BLM. (○) An impedance spectrum of a different nano-BLM preparation, three days after its formation. The solid lines are the results of the fitting procedure using the equivalent circuit shown in Fig. 4 *B*: (□) $C_m = 11.7$ nF, $R_m = 4.7$ GΩ; (○) $C_m = 17.2$ nF, $R_m = 0.35$ GΩ. (*B*) Equivalent circuit composed of a parallel *RC*-element (R_m and C_m) representing the electrical behavior of a lipid bilayer in series to an ohmic resistance R_{el} representing the electrolyte solution.

the self-assembled monolayer did not alter the impedance behavior. Only the ohmic resistance of the electrolyte was detected (Fig. 4 *A*). This result corroborates that the current only flows through the pores, and changes on top of the alumina pore columns cannot be detected. As the resistance R_{el} does not change after monolayer formation, it can also be concluded that all pores are still filled with electrolyte even though the surface is more hydrophobic on one side and that the inner walls of the pores are not covered with gold and a hydrophobic monolayer as that would prevent pore filling with an aqueous solution.

Subsequently, DPhPC dissolved in *n*-decane was spread on the functionalized porous alumina substrates resulting in a hydrophobic droplet with a thickness of several micrometers. The formation of lipid bilayers was followed by means of impedance spectroscopy in a frequency regime of 10^{-2}–10^{6} Hz. In Fig. 4 *A*, impedance spectra of functionalized porous alumina substrates before (*solid symbols*) and after addition (*open symbols*) of the lipid droplet are shown. Both impedance spectra after addition of the lipid droplet clearly indicate the formation of an insulating layer across the porous matrix. Control experiments, in which porous substrates were not functionalized with a DPPTE-monolayer, revealed that the insulating layer is only formed in the presence of a hydrophobic monolayer. The impedance spectrum (□) was recorded one day after formation of the nano-BLM and was used for single-channel measurements of gramicidin after impedance analysis. To extract membrane specific parameters from the impedance data, the simplest equivalent circuit to model the electrical behavior of a lipid bilayer was used, which is depicted in Fig. 4 *B*. It is composed of a parallel *RC*-element (R_m and C_m) representing the electrical behavior of a lipid bilayer in series to an ohmic resistance R_{el} representing the electrolyte solution. The obtained impedance spectrum is characterized by the electrolyte resistance R_{el} in the high-frequency regime (5×10^{4}–10^{6} Hz) and the capacitance C_m at frequencies below 5×10^{4} Hz. At frequencies below 3×10^{-1} Hz, a second ohmic resistance is discernable, which is attributed to the membrane resistance R_m. Fitting the parameters of the equivalent circuit shown in Fig. 4 *B* to the data presented in

Fig. 4 *A* results in good agreement between data and fit with a membrane capacitance of $C_m = 11.7$ nF and a membrane resistance of $R_m = 4.7$ GΩ. Although for all treated impedance data with this model C_m is well-defined in the spectrum with a fitting error of ~1–3%, the fit error of R_m depends on its absolute value. For membrane resistances >1 GΩ, the ohmic resistance is only determined within the frequency range of 10^{-2}–10^{-1} Hz resulting in a fit error of ~20%, whereas below 1 GΩ the fit error is <12%. The impedance spectrum (○) in Fig. 4 *A* represents a different membrane preparation and was monitored three days after nano-BLM formation. Even after three days, the impedance spectra clearly indicate the existence of an insulating nano-BLM with a membrane capacitance of $C_m = 17.2$ nF and a membrane resistance of $R_m = 0.35$ GΩ. Owing to the lower membrane resistance, the ohmic contribution is readily discernible at frequencies below 1 Hz. For more than 50 membrane preparations membrane capacitances with a mean value of 14.9 ± 3.3 nF were obtained. For the membrane resistance, such value cannot be given easily. Though each membrane preparation led to the formation of a nano-BLM with the characteristic membrane capacitance, the membrane resistance varied. The distribution of membrane resistances will be discussed in detail below.

Directly after applying the lipid droplet onto the functionalized porous surface, the obtained capacitance values are typically smaller. By continuously recording impedance spectra, changes in the electrical parameters of the formed layer can be followed time-resolved. A typical time-resolved change in capacitance is depicted in Fig. 5. The bilayer formation process starts at a capacitance of 4.3 nF and increases until it levels off at a stable capacitance value of 15.3 nF. The increase in capacitance can be attributed to a thinning process of the bilayer (Benz et al., 1975) and was observed for all membrane preparations ($n >$ 50). The thinning process takes ~10–35 min until a stable and constant membrane capacitance is reached.

To calculate an area-related capacitance value, the active area has to be determined. Since the current exclusively flows through the pores, only their area must be taken into account. One can roughly estimate the active area from the total solution exposed area (7 mm^2) and the porosity of the porous material. Taking the porosity of 33% for an alumina substrate anodized in phosphoric acid solution into account, an active area of $A = 2.3$ mm^2 is calculated. Thus, the mean capacitance of $C_m = 14.9 \pm 3.3$ nF translates into a specific capacitance of $C_m^A = 0.65 \pm 0.2\ \mu F/cm^2$. C_m^A is defined as $C_m A^{-1}$. This value agrees well with those obtained for classical black lipid membranes and supports the idea that single lipid bilayers have been formed across the pores. For the specific membrane resistance, maximum values of up to 1.6×10^8 Ω cm^2 were obtained for nano-BLMs bathed in 0.5 M KCl solution.

Long-term stability of nano-BLMs

The achieved membrane resistances of the nano-BLMs are similar to those of traditional BLMs and are obviously sufficient to perform single-channel recordings. However, the suitability of classical BLMs in biosensor applications is limited, as the BLM ruptures at a certain point, i.e., owing to mechanical distortion, in one single event leading to the loss of membrane resistance. In contrast, in nano-BLMs, each membrane suspending a single pore, is decoupled from the others and can thus rupture separately, which would result in a continuously decreasing membrane resistance. To prove this hypothesis, we investigated the change in membrane resistance by means of impedance spectroscopy time-resolved. In Fig. 6, R_m as a function of time is shown. In the first 48 h after membrane formation, R_m drops from 7 GΩ to 1 GΩ. During this time period, the membrane is well-suited for single-channel measurements. Then, the membrane resistance further decreases, leading to membrane resistances of ~150 MΩ after 72 h, 16 MΩ after 96 h, and 2 MΩ after 120 h. After 132 h, the membrane resistance has been reduced to 1 MΩ. The continuous decrease in membrane resistance supports the hypothesis that each membrane

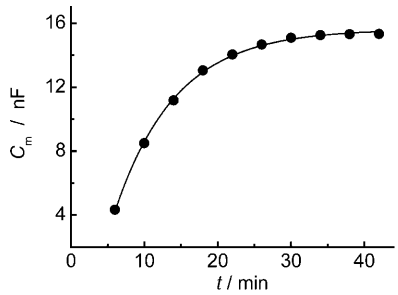

FIGURE 5 Time-dependent increase in capacitance C_m after its initial formation by painting a lipid droplet across the porous matrix. The membrane capacitance C_m increases from 4.3 nF to a final value of 15.3 nF. The solid line is the result of an asymptotical fit to the data and serves as a guide for the eye.

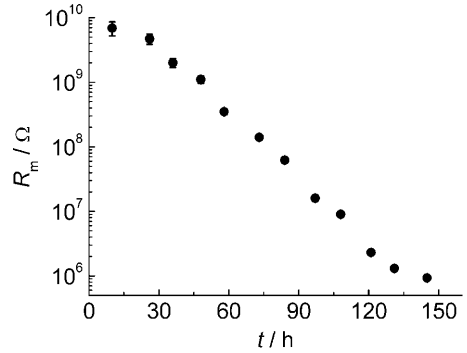

FIGURE 6 Time course of the membrane resistance R_m obtained by electrochemical impedance analysis of a nano-BLM in a frequency range of 10^{-2}–10^6 Hz. The membrane resistance was extracted from the impedance data by fitting the parameters of the equivalent circuit shown in Fig. 4 *B* to the data. Error bars indicate the error of the fit parameter R_m.

suspending a pore can rupture individually. From a statistical analysis of more than 30 membrane preparations the lifetime of the nano-BLM with membrane resistances >1 GΩ was calculated to be 1.5 ± 0.5 days; 2.5 ± 1 days for those with resistances >100 MΩ; 3.5 ± 1 for those >10 MΩ; and 4.5 ± 1.5 days for those >1 MΩ. After 5 ± 1.5 days, the membrane resistance decreases to values <1 MΩ. Notably, in some cases it occurred during the time course of the experiment that the membrane resistance increased again, which indicates that a self-healing process might occur within the membrane.

Impedance analysis of gramicidin D-doped nano-BLMs

Functionality of nano-BLMs can only be demonstrated by inserting channel-active peptides such as gramicidin or alamethicin. In particular, gramicidin is frequently used to support the idea of a single lipid bilayer, as the peptide is only active if the membrane is as thin as one lipid bilayer. To investigate the influence of gramicidin on the electrical behavior of nano-BLMs, we added the ion channel gramicidin to the electrolyte (0.1 M Na_2SO_4) on each side of the measuring chamber resulting in a final concentration of 10^{-8} M. By means of impedance spectroscopy as an integral method, peptide insertion and channel activity was followed. Here, a nano-BLM has been chosen that was not defect-free to be able to monitor the membrane resistance by impedance spectroscopy in the observed frequency range. Even though the nano-BLM was not defect-free, an increase in ion conductance was clearly observed (Fig. 7). Within 10 min after addition of the peptide, the membrane resistance was decreased from $R_m = 8.73$ MΩ to 5.45 MΩ. The membrane capacitance remained constant with a value of 13.1 nF.

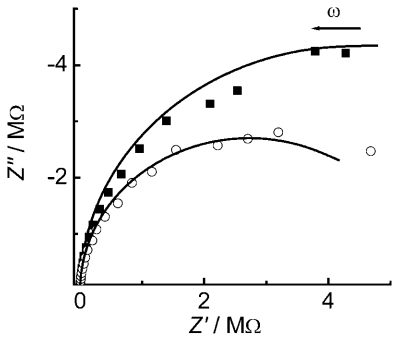

FIGURE 7 Impedance analysis of a nano-BLM bathed in 0.1 M Na_2SO_4 recorded in a frequency range of 10^{-1}–10^{6} Hz before (■) and after (○) gramicidin addition to the *cis* and *trans* compartment. The final gramicidin concentration was 10^{-8} M. After 10 min incubation time, the membrane resistance was dropped by $>3 \times 10^6$ Ω from $R_m = 8.73 \times 10^6$ Ω to $R_m = 5.45 \times 10^6$ Ω. The solid lines are the results of the fitting procedure with the equivalent circuit shown in Fig. 4 *B*.

Single-channel recording of gramicidin in nano-BLMs

If nano-BLMs have a high membrane resistance in the GΩ regime, they should be ideally suited for low noise electrical recording of transmembrane ion currents. Here, the general functionality of nano-BLMs was demonstrated using gramicidin as a channel-forming peptide. For single-channel measurements, nano-BLMs were bathed on either side in 0.5 M KCl. Application of a holding potential of $V_h = +70$ mV across the bilayer allowed the voltage-driven ion current induced by gramicidin upon its bilayer partition to be measured. Normally, gramicidin was added to both the *cis* and *trans* compartment of the nano-BLM, resulting in a final concentration of 10^{-8} M. Single conductance states and multiples of those were observed as shown in the representative current trace in Fig. 8 *A* ~10 min after gramicidin has been added to the solution. If gramicidin was added only to the *cis* side, the first conductance events were observed only after 1 h. The statistical distribution of conductance

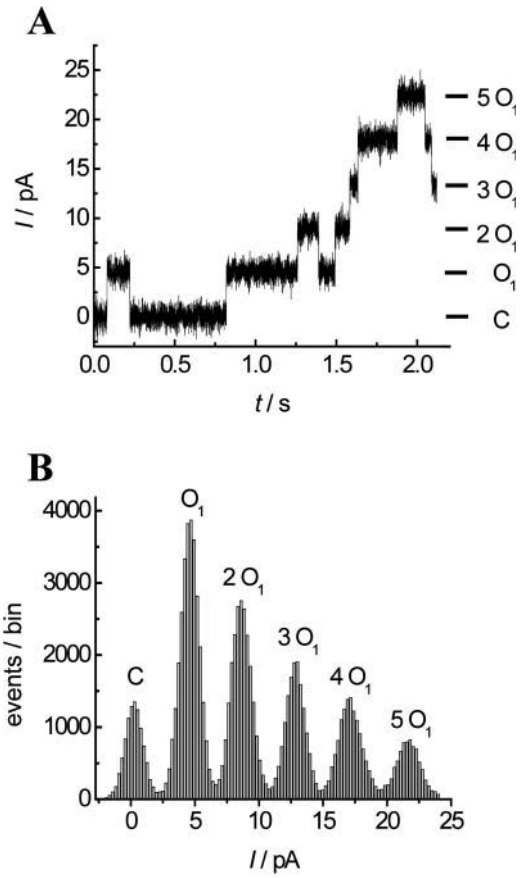

FIGURE 8 (*A*) Current trace of a nano-BLM after addition of gramicidin. The nano-BLM was symmetrically bathed in 0.5 M KCl and a holding potential of $V_h = 70$ mV was applied. Data were filtered at 1 kHz. Single and multichannel openings up to the fifth opening level ($5O_1$) were recorded: $C =$ 0.25 pA; $O_1 = 4.35$ pA; $2O_1 = 8.35$ pA; $3O_1 = 12.61$ pA; $4O_1 = 16.77$ pA; and $5O_1 = 21.45$ pA. (*B*) Corresponding current amplitude histogram.

states is shown in the histogram analysis in Fig. 8 *B*. Single-channel conductance states (O_1) as well as multiples of those with distinct conductance states up to the fifth opening level ($5O_1$) were recorded. A single open state O_1 exhibits a current flow of 4.2 ± 0.15 pA, which translates in a gated conductance state of 60 ± 2 pS. Using the same conditions, conductance measurements were also carried out in 0.5 M CsCl solution resulting in a slightly increased mean conductance of 76 ± 5 pS compared to that obtained in 0.5 M KCl solution. In 0.5 M LiCl, only single-channel openings (O_1) were observed, which occurred rather rarely with a mean conductance of 11 ± 2 pS.

Interestingly, the larger area of 7 mm^2 of the nano-BLM compared to a classical BLM with a typical area of 1 mm^2 does not influence the sensitivity of the measurement. The noise level is in the same range and is typically 2 pA (Fig. 8 *B*) for the closed state. Thus, the experiment clearly demonstrates the applicability of nano-BLMs for single channel recordings.

Single-channel recording of alamethicin in nano-BLMs

Alamethicin is known as a peptide that self-integrates into bilayers and forms voltage-gated ion channels of defined conductances by oligomerization. The nano-BLMs were bathed on both sides in 0.5 M KCl and alamethicin was added only to the *cis* side from an ethanolic solution resulting in a final concentration of $\sim 10^{-7}$ M while applying a holding potential of $V_h = +70$ mV. The voltage-dependent activation of single alamethicin channels with up to five conductance states was observed (Fig. 9, *A* and *B*). Induced by the applied positive potential, alamethicin channels appear as multilevel current bursts rising from the background current of 3 pA (closed state *C*) to conducting states of 420 pA (open state O_5). The pore can adopt several electrically distinct states, which are defined by the number of monomers making up the pore-forming aggregate. Discrete conductance states up to the fifth conductance level (O_5) can be clearly resolved. Each change in the pore state is due to the association or dissociation of an alamethicin monomer to an existing aggregate. Once an initial small channel has been formed, the conductance increases fast and in a stepwise manner.

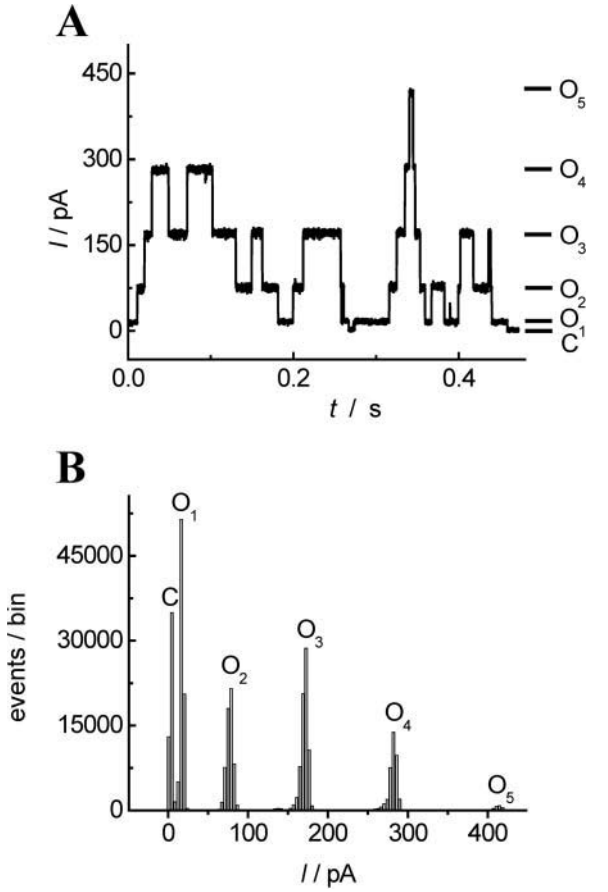

FIGURE 9 (*A*) Representative current trace showing single pore fluctuations induced by alamethicin. The nano-BLM was symmetrically bathed in 0.5 M KCl and a holding potential of $V_h = 70$ mV was applied. Data were filtered at 1 kHz. The whole burst of fluctuations is due to a single pore event, fluctuating between conductance levels O_1–O_5. $O_1 = 16.4$ pA; $O_2 = 79.1$ pA; $O_3 = 171.7$ pA; $O_4 = 281.6$ pA; and $O_5 = 415.2$ pA. $C = 3.0$ pA reflects the current baseline with the channel closed. (*B*) Corresponding current amplitude histogram.

DISCUSSION

The aim of this work was to obtain a membrane system that is attached to a solid support so that it can be applied in chip technology with the future perspective to obtain high-throughput screening assays and exhibits high membrane resistances to perform single-channel measurements. As solid supported membranes, on the one hand, are well-suited for chip-based biosensors, and black lipid membranes, on the other hand, exhibit high membrane resistances to allow for single-channel recordings, we aimed to combine the advantages of both membrane systems in one, which we call nano-BLMs (Fig. 10). To support lipid bilayers, porous alumina with a sieve-like structure was chosen. This material can be readily prepared in almost arbitrary lateral dimensions with large reproducibility and the pore size can be adjusted within a range of 15–420 nm (Li et al., 1998). The defined highly ordered pore structure and low surface roughness turned out to be advantageous for a reproducible quality of the nano-BLMs.

The selective functionalization of the upper surface of the porous alumina was a prerequisite for the formation of nano-BLMs. The hydrophobic DPPTE monolayer on top of the porous alumina surface favors the formation of suspending bilayers rather than a complete membrane coverage inside the pores as it was reported by Bourdillon and co-workers (Proux-Delrouyre et al., 2001). If the upper surface was not hydrophobic, lipid bilayer formation was

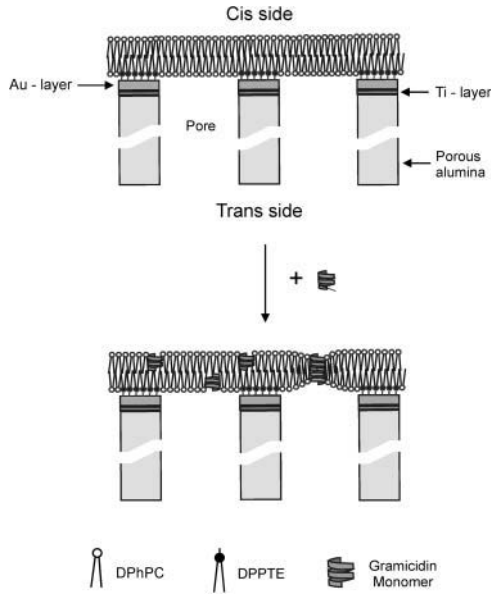

FIGURE 10 Schematic representation of a nano-BLM formed by DPhPC onto a self-assembled DPPTE monolayer chemisorbed on a gold-covered surface of an alumina substrate. The figure is not drawn to scale.

not observed. Every membrane preparation resulted in the formation of a nano-BLM as verified by impedance analysis. Impedance data were analyzed using the simplest equivalent circuit composed of a parallel *RC* circuit that describes the electrical behavior of a lipid membrane. Based on this model, a specific mean membrane capacitance of 0.65 $\pm$ 0.2 μF/cm^2 ($n > 50$) was obtained for the nano-BLMs onto the prefunctionalized porous alumina substrates. This value indicates that single lipid bilayers have been formed on the porous alumina substrates. The specific capacitance is consistent with those reported for classical BLMs formed across an aperture in a Teflon foil, which are typically $\sim$0.5 μF/cm^2 (Benz et al., 1975; Tien and Ottova, 2000). It is also consistent with specific capacitance values of lipid bilayers formed across an aperture of a micromachined support. Lipid membranes suspending apertures of 10–500 μm in diameter micromachined in silicon or glass chips were reported to exhibit specific capacitances of 0.3–1.1 μF/cm^2 (Cheng et al., 2001; Fertig et al., 2001; Pantoja et al., 2001; Peterman et al., 2002). Since impedance studies indicate that the current exclusively flows through the pores, the specific membrane capacitances of the nano-BLMs were calculated using the estimated porous area obtained from SEM images. Due to the error of the determined area, the specific capacitance and resistance values will have an error of $\sim$10%. Within this error, the determined capacitances are still in the same range as those reported for classical BLM preparations.

In contrast to C_m, the membrane resistance R_m of the nano-BLMs strongly depends on the quality of the preparation and the age of the nano-BLM. One out of four preparations was well-suited for long-term and low-noise single-channel recordings with a membrane resistance of >1 GΩ. Taking the actual area into account, specific membrane resistances of up to 1.6×10^8 Ω cm^2 were obtained for nano-BLMs bathed in 0.5 M KCl solution. For classical BLMs unbuffered in 0.1 M KCl electrolyte solutions, specific resistances of $\sim 10^8$ Ω cm^2 were reported (Benz et al., 1975; Tien and Ottova, 2000). Cheng et al. (2001) obtained specific membrane resistances of $\sim 10^7$ Ω cm^2 for a lipid bilayer suspending an aperture 128 μm in diameter, which was micromachined in gold/photoresist. However, for single-channel recording, not the specific membrane resistance but the absolute value of the membrane resistance is the decisive parameter. By decreasing the area, the resistance is increased. For example, Schmidt et al. (2000) reported a membrane resistance exceeding 10^9 Ω obtained from membranes suspending one single aperture micromachined in a silicon chip with diameters of 0.6–7 μm. The specific resistance is, however, only $\sim$5–400 Ω cm^2. For comparison, we obtained specific membrane resistances up to 1.6×10^8 Ω cm^2 on a total area of 7 mm^2 comprising $\sim$37 million pores each with a mean diameter of 280 nm.

A second interesting point concerning the membrane resistance is its time dependency. R_m continuously decreases over time (see Fig. 6). In the case of traditional BLMs and those more recently described based on apertures manufactured in silicon or glass supports, membrane rupture leads to a loss of membrane resistance in a single step. For example, conventional BLMs typically last no longer than 8 h (Tien and Ottova, 2000). Cheng et al. (2001) reported a stability of 5 h for a lipid membrane suspending an aperture 128 μm in diameter, whereas Schmidt et al. (2000) obtained a stability of $\sim$1 h for a lipid bilayer suspending a 0.6–7 μm hole in silicon. In the case of the nano-BLMs, each single membrane covering a pore of the porous alumina ruptures individually leading to a continuous decrease in R_m. Even four days after formation, a nano-BLM still exhibits specific membrane resistances of 4×10^5 Ω cm^2, which is in the same range as those of solid supported membranes. For example, for lipid bilayers immobilized on semiconductor and gold surfaces, Wiegand et al. (2002) reported resistances ranging between 10^3 and 10^5 Ω cm^2, whereas Purrucker et al. (2001) achieved membrane resistances up to 10^6 Ω cm^2. These solid supported membranes are typically stable for several days.

The continuous decrease in membrane resistance of the nano-BLMs indicates that a defect occurring at one site does not influence the stability of the entire membrane, i.e., a membrane suspending a single pore is decoupled from the others. Thus, scanning-electrochemical methods such as scanning ion conductance microscopy or scanning electrochemical microscopy exhibiting lateral resolutions in the range of 10–100 nm would allow addressing each membrane-suspended pore individually. Then, one would be able to measure on a membrane preparation even if some of the membranes suspending the pores are ruptured.

The biomimetic properties and suitability of nano-BLMs for the development of biosensors have been checked and

evaluated by monitoring the channel activity of gramicidin D and alamethicin. In case of gramicidin D, formation of the conducting dimer was followed by means of impedance spectroscopy and single-channel recording. Impedance recordings clearly demonstrated that the membrane resistance is decreased by $3 \times 10^6\ \Omega$ due to incorporation of conducting gramicidin dimers into nano-BLMs bathed in 0.1 M Na_2SO_4. Similar decreases in membrane resistances observed by means of impedance spectroscopy was already reported for solid supported membranes (Alonso-Romanowski et al., 1995; Gassa et al., 1997; Steinem et al., 1997; Vallejo and Gervasi, 2002). For solid supported membranes it is not feasible to monitor single-channel events after insertion of a membrane-active channel peptide. This can, however, be realized by using nano-BLMs. Bathed in 0.5 M KCl electrolyte solution, the different opening states of individual channels (O_1–$5O_1$) were clearly discernable, corroborating the idea that single lipid bilayers have been formed on the porous support as it is well-established that gramicidin ion channels can only be observed in single lipid bilayers. The mean conductance of ~60 pS applying a holding potential of 70 mV is in the conductance range reported by others (Andersen, 1983; Bamberg and Benz, 1976; Bamberg et al., 1976; Hladky and Haydon, 1972; Myers and Haydon, 1972). No channel activity was observed before adding the peptide to the solution. The specificity of gramicidin ion channels was proved by using CsCl and LiCl in addition to KCl as bathing solution. The larger conductance in case of Cs^+ cations and the decreased conductance of Li^+ cations are in line with the reported selectivity of gramicidin channels for monovalent cations, which is reported to be $Cs^+ > K^+ \gg Li^+$ (sequence of conductance) (Myers and Haydon, 1972) and confirms that the observed single-channel events are the result of gramicidin insertion. We calculated a mean channel lifetime of 412 ms based on opening and closing times of gramicidin pores from 40 ms up to 1.7 s. These values are in good agreement with those obtained for traditional BLM (Hladky and Haydon, 1972). Restricted diffusion of gramicidin in the *trans* layer does not influence the gating kinetics. Notable, however, is the observation that the first channel openings typically occur 10 min after adding ethanolic gramicidin solution to both the *cis* and *trans* compartment. If gramicidin was added only to the *cis* compartment, the first channel events were recorded after a time period of >1 h due to restricted diffusion of gramicidin within the pores.

In contrast to gramicidin D, which inserts into bilayers without the application of a potential, a potential difference across the bilayer needs to be applied for the insertion of the peptide alamethicin. Here, no notable channel activity of alamethicin was observed applying electrical potentials between −30 mV and +50 mV indicating the voltage-gating nature of alamethicin channels. Applying a potential of +70 mV results in current fluctuations, which appear in bursts with different conductance levels (O_1–O_5) ranging between 0.2 and 6 nS. The lower conductance states occurred more frequently. The different conductance levels are explained by the scenario that the peptide self-assembles into α-helical bundles forming a pore. The number of helices that participate in the pore forming process varies between 4 and 11 (Sansom, 1991) leading to different pore sizes and thus, to different conductance levels. The obtained conductance values of alamethicin pore formation in nano-BLMs are in reasonably good agreement with data reported in literature (Gordon and Haydon, 1976; Hall et al., 1984; Sansom, 1991; Vodyanoy et al., 1983).

CONCLUSIONS

Nano-BLMs are a hybrid system combining classical BLMs with solid supported membranes, and appear to be well-suited for the development of membrane biosensors with fully functional transmembrane ion channels. As these membranes are attached to a solid support, they can be applied in chip technology, and this will be an interesting tool for the establishment of high-throughput screening assays based on membrane-confined proteins. Furthermore, the highly ordered porous structure serving as membrane support will allow addressing each single substrate pore by space-resolved electrochemical techniques. This will enable one to perform several measurements on one support quasi-simultaneously.

We thank R. Wehrspohn and K. Nielsch for valuable input concerning the porous materials.

The work was supported by the Bundesministerium für Bildung und Forschung within the nanobiotechnology project.

REFERENCES

Alonso-Romanowski, S., L. M. Gassa, and J. R. Vilche. 1995. An investigation by EIS of gramicidin channels in bilayer lipid membranes. *Electrochim. Acta*. 40:1561–1567.

Andersen, O. S. 1983. Ion movement through gramicidin A channels. *Biophys. J*. 41:119–133.

Andreou, V. G., and D. P. Nikolis. 1998. Flow injection monitoring of aflatoxin M1 in milk and milk preparations using filter-supported bilayer lipid membranes. *Anal. Chem*. 70:2366–2371.

Bamberg, E., and R. Benz. 1976. Voltage-induced thickness changes of lipid bilayer membranes and the effect of an electric field on gramicidin A channel formation. *Biochim. Biophys. Acta*. 426:570–580.

Bamberg, E., K. Noda, E. Gross, and P. Läuger. 1976. Single-channel parameters of gramicidin A, B, and C. *Biochim. Biophys. Acta*. 419:223–228.

Baumgart, T., M. Kreiter, H. Lauer, R. Naumann, G. Jung, A. Jonczyk, A. Offenhäusser, and W. Knoll. 2003. Fusion of small unilamellar vesicles onto laterally mixed self-assembled monolayers of thiolipopeptides. *J. Colloid Interface Sci*. 258:298–309.

Benz, R., O. Fröhlich, P. Lauger, and M. Montal. 1975. Electrical capacity of black lipid films and of lipid bilayers made from monolayers. *Biochim. Biophys. Acta*. 394:323–334.

Cheng, Y., R. J. Bushby, S. D. Evans, P. F. Knowles, R. E. Miles, and S. D. Ogier. 2001. Single ion channel sensitivity in suspended bilayers on micromachined supports. *Langmuir*. 17:1240–1242.

de Laet, J., H. Teeryn, and J. Vereecken. 1995. The use of impedance spectroscopy and optical reflection spectroscopy to study modified aluminum surfaces. *Electrochim. Acta.* 7:1155–1161.

Favero, G., L. Campanella, A. D'Annibale, R. Santucci, and T. Ferri. 2003. Mixed hybrid bilayer lipid membrane incorporating valinomycin: improvements in preparation and functioning. *Microchem. J.* 74:141–148.

Favero, G., A. D'Annibale, L. Campanella, R. Santucci, and T. Ferri. 2002. Membrane supported bilayer lipid membranes array: preparation, stability, and ion-channel insertion. *Anal. Chim. Acta.* 460:23–34.

Fertig, N., C. Meyer, R. H. Blick, C. Trautmann, and J. C. Behrends. 2001. Microstructured glass chip for ion-channel electrophysiology. *Phys. Rev. E. Stat. Nonlin. Soft Matter Phys.* 64:1–4.

Gassa, L. M., A. E. Vallejo, S. Alonso-Romanowski, and J. R. Vilche. 1997. Identification of channel membrane processes in bilayer lipid membranes by electrochemical techniques. *Bioelectrochem. Bioenerg.* 42:187–192.

Gordon, L. G. M., and D. A. Haydon. 1976. Kinetics and stability of alamethicin conducting channels in lipid bilayers. *Biochim. Biophys. Acta.* 436:541–556.

Hall, J. E., I. Vodyanoy, T. M. Balasubramanian, and G. R. Marshall. 1984. Alamethicin. A rich model for channel behavior. *Biophys. J.* 45:233–247.

Hanke, W., and W. R. Schlue. 1993. Planar Lipid Bilayers: Methods and Applications. Academic Press, London.

Hladky, S. B., and D. A. Haydon. 1972. Ion transfer across lipid membranes in the presence of gramicidin A. I. Studies of the unit conductance channel. *Biochim. Biophys. Acta.* 274:294–312.

Jessensky, O., F. Müller, and U. Gösele. 1998. Self-organized formation of hexagonal pore arrays in anodic alumina. *Appl. Phys. Lett.* 72:1173–1175.

Li, A. P., F. Müller, A. Birner, K. Nielsch, and U. Gösele. 1998. Hexagonal pore arrays with a 50–420 nm interpore distance formed by self-organization in anodic alumina. *J. Appl. Phys.* 84:6023–6026.

Li, A. P., F. Müller, A. Birner, K. Nielsch, and U. Gösele. 1999a. Fabrication and microstructuring of hexagonally ordered two-dimensional nanopore arrays in anodic alumina. *Adv. Mater.* 11:483–487.

Li, A. P., F. Müller, A. Birner, K. Nielsch, and U. Gösele. 1999b. Polycrystalline nanopore arrays with hexagonal ordering on aluminum. *J. Vac. Sci. Technol. A.* 17:1428–1431.

Mueller, P., D. O. Rudin, H. T. Tien, and W. C. Wescott. 1963. Methods for the formation of single bimolecular lipid membranes in aqueous solutions. *J. Phys. Chem.* 67:534–535.

Myers, V. B., and D. A. Haydon. 1972. Ion transfer across lipid membranes in the presence of gramicidin A. II. The ion selectivity. *Biochim. Biophys. Acta.* 274:313–322.

Naumann, R., T. Baumgart, P. Graber, A. Jonczyk, A. Offenhäusser, and W. Knoll. 2002. Proton transport through a peptide-tethered bilayer lipid membrane by the H^+-ATP synthase from chloroplasts measured by impedance spectroscopy. *Biosens. Bioelectron.* 17:25–34.

Nielsch, K., J. Choi, K. Schwirn, R. B. Wehrspohn, and U. Gösele. 2002. Self-ordering regimes of porous alumina: the 10% porosity rule. *Nano Lett.* 2:677–680.

Nikolelis, D. P., and C. G. Siontorou. 1995. Bilayer lipid membranes for flow injection monitoring of acetylcholine, urea, and penicillin. *Anal. Chem.* 67:936–944.

Ogier, S. D., R. J. Bushby, Y. Cheng, S. D. Evans, S. W. Evans, T. A. Jenkins, P. F. Knowles, and R. E. Miles. 2000. Suspended planar phospholipid bilayers on micromachined supports. *Langmuir.* 16:5696–5701.

Osborn, T. D., and P. Yager. 1995. Formation of planar solvent-free phospholipid bilayers by Langmuir-Blodgett transfer of monolayers to micromachined apertures in silicon. *Langmuir.* 11:8–12.

Pantoja, R., D. Sigg, R. Blunck, F. Bezanilla, and J. R. Heath. 2001. Bilayer reconstitution of voltage-dependent ion channels using a microfabricated silicon chip. *Biophys. J.* 81:2389–2394.

Peterman, M. C., J. M. Ziebarth, O. Braha, H. Bayley, H. A. Fishman, and D. M. Bloom. 2002. Ion channels and lipid bilayer membranes under high potential using microfabricated apertures. *Biomed. Microdevices.* 4:231–236.

Proux-Delrouyre, V., J. M. Laval, and C. Bourdillon. 2001. Formation of streptavidin-supported lipid bilayers on porous anodic alumina: electrochemical monitoring of triggered vesicle fusion. *J. Am. Chem. Soc.* 123:9176–9177.

Purrucker, O., H. Hillebrandt, K. Adlkofer, and M. Tanaka. 2001. Deposition of highly resistive lipid bilayers on silicon-silicon dioxide electrode and incorporation of gramicidin studied by AC impedance spectroscopy. *Electrochim. Acta.* 47:791–798.

Raguse, B., V. Braach-Maksvytis, B. A. Cornell, L. G. King, P. D. J. Osman, R. J. Pace, and L. Wieczorek. 1998. Tethered lipid bilayer membranes: formation and ionic reservoir characterization. *Langmuir.* 14:648–659.

Sackmann, E. 1996. Supported membranes: scientific and practical applications. *Science.* 271:43–48.

Sackmann, E., and M. Tanaka. 2000. Supported membranes on soft polymer cushions: fabrication, characterization, and applications. *Trends Biotechnol.* 18:58–64.

Sansom, M. S. P. 1991. The biophysics of peptide models of ion channels. *Prog. Biophys. Mol. Biol.* 55:139–235.

Schmidt, C., M. Mayer, and H. Vogel. 2000. A chip-based biosensor for the functional analysis of single ion channels. *Angew. Chem. Int. Edit.* 39:3137–3140.

Sengupta, E., J. Schilling, S. Marx, M. Fischer, A. Bacher, and E. Sackmann. 2003. Mimicking tissue surfaces by supported membrane coupled ultrathin layer of hyaluronic acid. *Langmuir.* 19:1775–1781.

Steinem, C., A. Janshoff, H.-J. Galla, and M. Sieber. 1997. Impedance analysis of ion transport through gramicidin channels incorporated in solid supported lipid bilayers. *Bioelectrochem. Bioenerg.* 42:213–220.

Steinem, C., A. Janshoff, W.-P. Ulrich, M. Sieber, and H.-J. Galla. 1996. Impedance analysis of supported lipid bilayer membranes: a scrutiny of different preparation techniques. *Biochim. Biophys. Acta.* 1279:169–180.

Stora, T., J. H. Lakey, and H. Vogel. 1999. Ion-channel gating in transmembrane receptor proteins: functional activity in tethered lipid membranes. *Angew. Chem. Int. Edit.* 38:389–392.

Terrettaz, S., M. Mayer, and H. Vogel. 2003. Highly electrically insulation tethered lipid bilayers for probing the function of channel proteins. *Langmuir.* 19:5567–5569.

Tien, H. T., and A. L. Ottova. 1998. Supported planar lipid bilayers (s-BLM) as electrochemical biosensors. *Electrochim. Acta.* 43:3587–3610.

Tien, H. T., and A. L. Ottova. 2000. Membrane Biophysics: Planar Lipid Bilayers and Spherical Liposomes. Elsevier, Amsterdam and New York.

Vallejo, A. E., and C. A. Gervasi. 2002. Impedance analysis of ion transport through gramicidin channels in supported lipid bilayers. *Bioelectrochemistry.* 57:1–7.

Vodyanoy, I., J. E. Hall, and T. M. Balasubramanian. 1983. Alamethicin-induced current-voltage curve asymmetry in lipid bilayers. *Biophys. J.* 42:71–82.

Wiegand, G., N. Arribas-Layton, H. Hillebrandt, E. Sackmann, and P. Wagner. 2002. Electrical properties of supported lipid bilayer membranes. *J. Phys. Chem. B.* 106:4245–4254.